MANUFACTURING AND CHARACTERIZATION OF GRID COMPOSITES

Sumit Kumar Das, Yash Chandrakant Salunke*, Dr. K. Vijay Kumar**, Dr. C. Ramesh**

** School of Aeronautical Sciences, Hindustan Institute of Technology and Science, Chennai-603103*
***Aerospace Composite Division, Chief Manager of Light Combat Helicopter (LCH), Hindustan Aeronautics Limited (HAL), Bangalore-*

KEYWORDS

Grid-stiffened composites
Carbon fiber
Glass fiber
Prepreg autoclave curing
Interlaminar shear strength (ILSS)
Flexural strength
Aerospace applications

ABSTRACT

Traditional composite materials, widely used in aerospace structures for their high strength-to-weight ratio, exhibit limitations such as delamination, inefficient load distribution, and limited damage tolerance, which can compromise structural integrity under operational stresses. Furthermore, conventional laminates often necessitate excessive material usage, leading to increased weight and manufacturing costs, thereby diminishing their efficiency in aerospace applications.

To address these challenges, grid-stiffened composites have been developed as an advanced alternative, offering enhanced mechanical performance through optimized structural design. This study investigates the fabrication and mechanical characterization of carbon and glass fiber-reinforced grid-stiffened composites produced via a prepreg-based autoclave curing process. Multiple grid configurations—including 0°, 45°, 90°, iso-grid (±45°), and plain lamina—were evaluated under tensile, flexural, and shear loading conditions to assess their structural performance.

Experimental analysis of 18 test specimens demonstrated that grid-stiffened composites exhibit an 18% improvement in strength-to-weight ratio compared to traditional laminates. The optimized grid configurations enhanced load distribution, improved damage tolerance, and reduced material consumption while maintaining structural integrity. These results highlight the potential of grid-stiffened composites for aerospace applications, such as aircraft fuselages, UAV components, and next-generation lightweight airframes. Their superior structural efficiency, combined with weight reduction and increased durability, positions them as a promising solution for advancing aerospace engineering and supporting sustainable aviation technologies.

1 Introduction

The aerospace industry has witnessed a giant transformation in material choice over current a long time, pushed by the demand for light-weight, high-electricity, and durable substances. whilst traditional steel alloys have been extensively used, they're more and more being replaced via superior composite substances due to their extremely good electricity-to-weight ratios, resistance to corrosion, and design flexibility. amongst these, fiber-bolstered polymer (FRP) composites have end up the material of desire for crucial aerospace additives along with aircraft wings, fuselage panels, and rotor blades . however, notwithstanding their significant adoption, conventional composite laminates aren't without limitations. demanding situations including bad interlaminar shear resistance, localized pressure concentrations, and susceptibility to delamination beneath dynamic loading situations have raised issues about their long-term structural integrity .

Corresponding Author: Sumit Kumar Das, Email: sumitdassbbsindigo@gmail.com

To address those obstacles, grid-stiffened composites have emerged as a revolutionary answer. those advanced substances include reinforcement patterns—including ortho-grid, iso-grid, and different geometric configurations—into the composite laminate shape. with the aid of doing so, they beautify load distribution, improve harm tolerance, and optimize stiffness-to-weight ratios. The concept of grid-stiffened composites changed into first advanced by way of NASA in the Nineteen Nineties for use in spacecraft and high-performance structural packages. on the grounds that then, they have got won substantial attention in the aviation and protection sectors due to their capability to lessen structural weight without compromising mechanical overall performance.

in contrast to traditional laminates, which depend upon uniform stacking sequences, grid-stiffened composites permit for tailored stiffness and electricity through strategic fiber orientation. This design technique reduces strain concentrations and improves resistance to interlaminar shear failure, a commonplace failure mode in traditional composites. moreover, grid-stiffened designs offer more suitable power absorption abilities, making them best for effect-resistant programs along with unmanned aerial automobiles (UAVs) and military plane.

Notwithstanding their potential, the mechanical overall performance of grid-stiffened composites below diverse loading conditions remains underexplored. whilst previous studies have centered on man or woman grid configurations, there is a lack of complete studies comparing the overall performance of carbon and glass fiber composites throughout more than one orientation. moreover, the relationship between grid architecture and failure mechanisms—such as matrix cracking, delamination, and fiber pull-out—has not been completely characterized. This expertise hole limits the ability of aerospace engineers to optimize grid-stiffened designs for unique applications, which include plane fuselage panels, wing structures, and rotor blades.

This has a look at targets to address these gaps with the aid of systematically investigating the mechanical behavior of carbon and glass fiber-strengthened grid composites with six distinct orientations: 0°, 45°, 90°, 0°/90°, iso-grid (±45°), and plain laminates. The studies goals are as follows:

- Fabrication: Manufacture grid-stiffened composites the usage of prepreg-based totally autoclave curing, ensuring disorder-loose laminates with precise fiber alignment.
- Mechanical testing: Quantify interlaminar shear strength (ILSS) and flexural properties through standardized assessments, such as brief-beam shear and 3-factor bending.
- Failure evaluation: Correlate grid structure with failure mechanisms using excessive-resolution microscopic imaging.
- Validation: evaluate experimental outcomes with theoretical models to refine predictive frameworks for grid-stiffened composites.

The findings of this take a look at have widespread implications for the aerospace enterprise, particularly inside the context of India's "Atmanirbhar Bharat" (Self-Reliant India) initiative. by advancing indigenous composite technologies, this study aligns with Hindustan Aeronautics restrained (HAL)'s task to broaden subsequent-technology aerospace components which might be lightweight, durable, and cost-powerful. furthermore, the insights won from this have a look at can inform the layout of grid-stiffened composites for a huge range of programs, from business aircraft to area exploration motors.

In precis, this study bridges the gap between conventional composite laminates and superior grid-stiffened designs, supplying a roadmap for optimizing structural efficiency and harm tolerance in aerospace applications. by using addressing the restrictions of conventional composites and leveraging the specific benefits of grid architectures, this looks at contributes to the ongoing evolution of aerospace substances and technology.

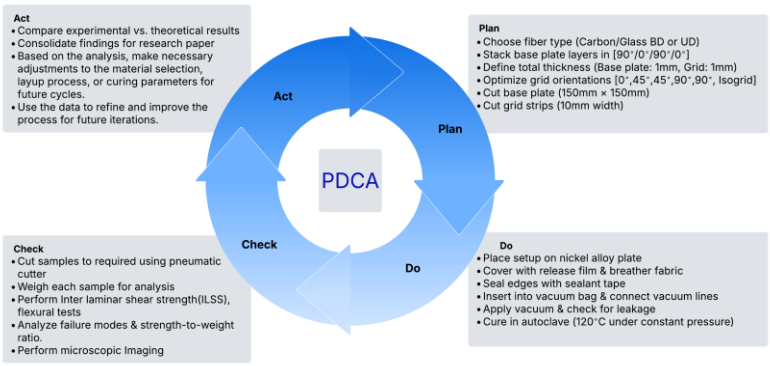

Fig 1: PDCA of the project

2 Material Selection and Methodology

The research methodology adopted in this study is designed to systematically investigate the mechanical behavior of grid-stiffened composites under various loading conditions. The methodology encompasses material selection, fabrication, mechanical testing, and failure analysis, ensuring a comprehensive evaluation of the composites' performance. Below is the PDCA methodology used:

2.1 Material Selection

The selection of material is a critical step in the improvement of composite systems, because it immediately impacts their mechanical performance, sturdiness, and suitability for specific programs. For this look at, carbon fiber-strengthened polymer (CFRP) and glass fiber-strengthened polymer (GFRP) prepregs were selected due to their

Corresponding Author: Sumit Kumar Das, Email: sumitdassbbsindigo@gmail.com

properly-hooked up use in aerospace programs and their complementary residences.

2.1.1 Carbon Prepregs

Carbon fiber prepregs (carbon 963 bi-directional and HTA7 uni-directional) were selected for their exceptional strength-to-weight ratio, high stiffness, and superior thermal stability. These properties make them ideal for primary load-bearing structures such as aircraft wings, fuselage panels, and rotor blades. The carbon fiber prepregs used in this study consist of continuous carbon fibers impregnated with an epoxy resin matrix, ensuring uniform resin distribution and enhanced mechanical properties.

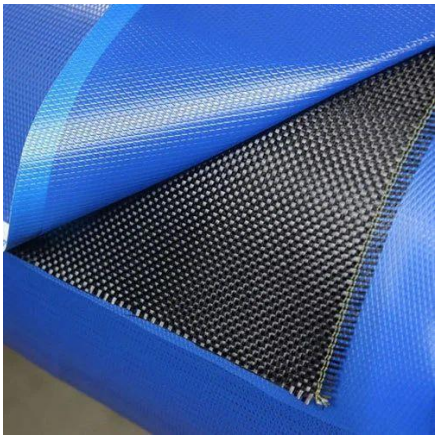

Fig 2: Carbon Prepreg sheet

2.1.2 Glass Prepregs

Glass fiber prepregs (glass 7781 bi-directional and 9756 uni-directional) were chosen for their moderate tensile strength, good flexibility, and cost-effectiveness. These properties make them suitable for secondary structures such as fairings, radomes, and interior components. The glass fiber prepregs used in this study are composed of silica-based fibers impregnated with an epoxy resin matrix.

Fig 3: Carbon Prepreg sheet

Property	Carbon Fiber Prepreg	Glass Fiber Prepreg
Tensile Strength (MPa)	4000	2500
Density (g/cm³)	1.75	2.5
Elongation (%)	1.5	4–5
Thermal Conductivity (W/m·K)	1.0	0.4

Table 1: Comparative properties of carbon and glass fiber prepregs

2.2 Methodology

The layup mold is cleaned and coated with a release agent (Teflon/PVA) to prevent adhesion. Prepreg sheets are thawed from -18°C for 2-3 hours, cut, and stacked in specified orientations (0°, 45°, 90°, Iso-grid). Each layer is placed on the mold, debulked, and covered with breather fabric and perforated release film before sealing in a vacuum bag (~0.8 bar). The laminate is cured in an autoclave, gradually heated from 23°C to 130°C, with dwell times of 45 min at 75°C and 1 hour at 130°C, then cooled to room temperature. Finally, the cured laminate is inspected for defects, voids, and delamination.

2.2.1 Cutting Process

The cured laminate panels are cut to standardized dimensions for mechanical testing. Specimen dimensions are designed in AutoCAD to ensure precision and compliance with ASTM standards. For interlaminar shear strength (ILSS) testing, specimens are cut to (10 × 20 mm) dimensions, while flexural test specimens are cut to (100 × 10 mm). A pneumatic cutter, powered by compressed air at 6 bar, is used to cut the panels.

3 Derivations and theoretical calculations

3.1 Bending Stiffness

The bending stiffness (D) quantifies a structure's resistance to bending moments. For grid-stiffened composites, it is derived by combining classical lamination theory with stiffener contribution. The bending stiffness (D_{lam}) of a conventional composite laminate is derived from Classical Lamination Theory (CLT).

For a plate under bending, the strain at any point z from the midplane is:

$$\epsilon_x = \epsilon_x^0 + zk_x, \qquad \epsilon_y = \epsilon_y^0 + zk_y, \qquad \gamma_{xy} = \gamma_{xy}^0 + zk_{xy}$$

where:

- ϵ_x^0, ϵ_y^0, γ_{xy}: Midplane strains.
- k_x, k_y, k_{xy}: Curvatures (bending and twisting).

The stiffness matrix Q of a unidirectional composite layer in global coordinates is:

$$Q_{ij} = \begin{bmatrix} Q_{11} & Q_{12} & Q_{16} \\ Q_{12} & Q_{22} & Q_{26} \\ Q_{16} & Q_{26} & Q_{66} \end{bmatrix}$$

Stress in the k-th ply is related to strain via the transformed reduced stiffness matrix $\bar{Q}_k$:

$$\begin{bmatrix} \sigma_x \\ \sigma_y \\ \tau_{xy} \end{bmatrix} = \bar{Q}_k \begin{bmatrix} \epsilon_x \\ \epsilon_y \\ \gamma_{xy} \end{bmatrix} = \bar{Q}_k \left(\begin{bmatrix} \epsilon_x^0 \\ \epsilon_y^0 \\ \gamma_{xy}^0 \end{bmatrix} + z \begin{bmatrix} k_x \\ k_y \\ k_{xy} \end{bmatrix} \right)$$

The force per unit length (N) and moment per unit length (M) are integrals of stress through the thickness:

$$\begin{bmatrix} N_x \\ N_y \\ N_{xy} \end{bmatrix} = \int_{-t/2}^{t/2} \begin{bmatrix} \sigma_x \\ \sigma_y \\ \tau_{xy} \end{bmatrix} dz, \begin{bmatrix} M_x \\ M_y \\ M_{xy} \end{bmatrix} = \int_{-t/2}^{t/2} \begin{bmatrix} \sigma_x \\ \sigma_y \\ \tau_{xy} \end{bmatrix} z dz$$

For a symmetric laminate (no bending-extension coupling):

- Midplane strains $\epsilon 0$ produce only forces (N).

Corresponding Author: Sumit Kumar Das, Email: sumitdassbbsindigo@gmail.com

- Curvatures κ produce only moments (M).

Thus, the moment-curvature relationship is:

$$\begin{bmatrix} M_x \\ M_y \\ M_{xy} \end{bmatrix} = \begin{bmatrix} D_{11} & D_{12} & D_{16} \\ D_{12} & D_{22} & D_{26} \\ D_{16} & D_{26} & D_{66} \end{bmatrix} \begin{bmatrix} k_x \\ k_y \\ k_{xy} \end{bmatrix}$$

Where D_{ij} are the bending stiffness coefficients.

The moment M_x is:

$$M_x = \int_{-t/2}^{t/2} \sigma_x \, z dz = \sum_{k=1}^{N} \int_{z_{k-1}}^{z_k} (\bar{Q}_{11}\epsilon_x + \bar{Q}_{12}\epsilon_y + \bar{Q}_{16}\gamma_{xy}) z dz$$

Substitute strains $\epsilon_x = zk_x,\ \epsilon_y = zk_y,\ \gamma_{xy} = z\,k_{xy}$

$$M_x = \sum_{k=1}^{N} (\bar{Q}_{11}k_x + \bar{Q}_{12}k_y + \bar{Q}_{16}k_{xy}) \int_{z_{k-1}}^{z_k} z^2 dz$$

$$\int_{z_{k-1}}^{z_k} z^2 dz = \frac{1}{3}(z_k^3 - z_{k-1}^3)$$

$$\boxed{D_{lam} = \frac{1}{3}\sum_{k=1}^{N} (\bar{Q}_{ij})\, k(Z_k^3 - Z_{k-1}^3)}$$

The distance from neutral axis is computed as:

$$z_{neutral} = \frac{t_b z_b + t_g z_g}{t_b + t_g}$$

For the base plate, using the standard bending stiffness formula:

$$D_{base} = \frac{E t_b^3}{12(1 - \vartheta^2)}$$

For the grid, the bending stiffness in the x and y directions depends on the grid width:

$$D_{grid} = \frac{E w t_g^3}{12(1 - \vartheta^2)}$$

$$D_{total} = D_{base} + D_{grid}$$

$$\boxed{D_{total} = \frac{E t_b^3}{12(1 - \vartheta^2)} + \frac{E w t_g^3}{12(1 - \vartheta^2)}}$$

3.2 ILSS (Interlaminar Shear Strength)

Interlaminar Shear Stress (τ) occurs when adjacent layers of a composite slide relative to each other. For a conventional laminate, this is resisted only by the matrix (e.g., epoxy). For grid-stiffened composites, fibers in the ribs provide additional shear resistance.

For a homogeneous laminate, ILSS is given by:

$$\tau_{max} = \frac{3P_{max}}{4bh}$$

Grid-stiffened composites resist shear through:

1. Matrix contribution (τ_m).
2. Fiber reinforcement from grids.

Fibers in grids experience axial stress $\sigma_f = E_f \epsilon_f$
The stress has a shear component based on grid angle θ:

$$\tau_f = \sigma_f sin\Theta cos\Theta$$

Cross-sectional area: $A_{grid} = w t_{grid}$

Fiber volume fraction: V_f

Shear force carried by fibers: $F_{fiber} = \sigma_f . (V_f A_{grid}) . sin\Theta cos\Theta$

Shear per Unit Area:

$$ILSS_{fiber} = \frac{F_{finer}}{s.w} = \frac{\sigma_f V_f t_{grid} sin\Theta cos\Theta}{s}$$

Combine matrix and fiber terms:

$$\boxed{ILSS_{fiber} = \tau_m + \frac{\sigma_f V_f t_{grid} sin\Theta cos\Theta}{s}}$$

4 Testing and analysis

The mechanical performance of grid-stiffened composites was evaluated through standardized tests, including interlaminar shear strength (ILSS) and flexural testing. These tests were conducted to quantify the composites' resistance to shear and bending stresses, respectively, and to analyze their failure mechanisms.

4.1 Interlaminar Shear Strength (ILSS) Testing

ILSS checking out turned into finished the usage of a common trying out machine (UTM) in accordance with ADS26. The take a look at setup covered a 3-factor bending fixture with cylindrical helps to preserve the specimen. The specimen dimensions were 10 mm (width) × 20 mm (length) × 2 mm (thickness), with a span-to-thickness ratio of 5:1. The test became performed at a loading speed of 2 mm/min till failure.

The most load at failure (Pmax) become recorded, and the ILSS became calculated using the formula:

$$\tau_{max} = \frac{3P}{4bh}$$

4.2 Flexural Test

Flexural testing was conducted using a three-point bending setup in accordance with ADS29. The specimen dimensions were 100 mm (length) × 10 mm (width) × 2 mm (thickness), with a span length of 80 mm. The load was applied at the midpoint of the specimen at a rate of 2 mm/min until failure occurred:

$$\sigma = \frac{3PL}{2bh^2}$$

Corresponding Author: Sumit Kumar Das, Email: sumitdassbbsindigo@gmail.com

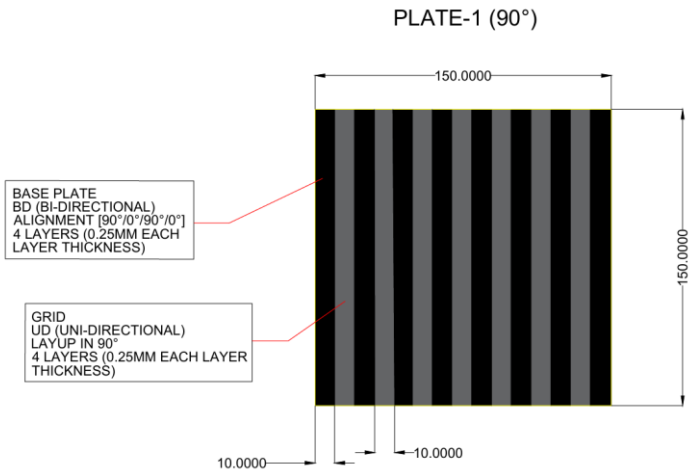

(a)

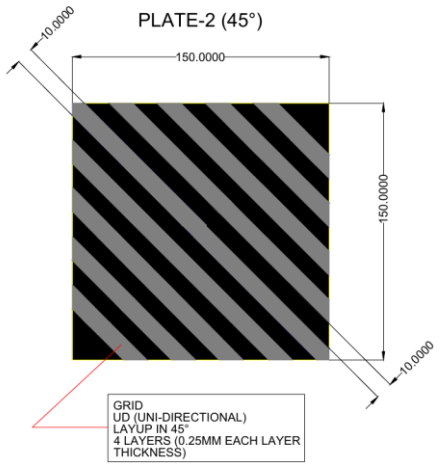

(b)

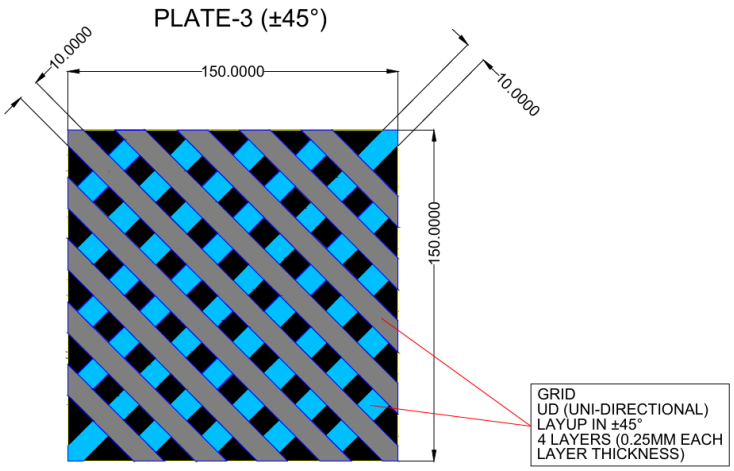

(c)

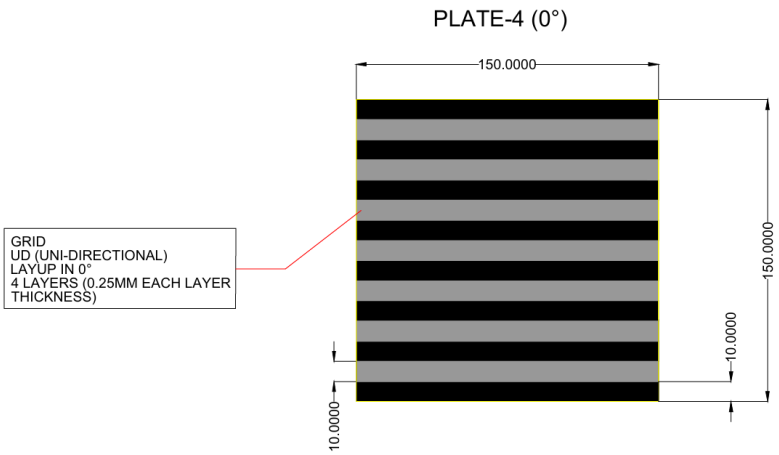

(d)

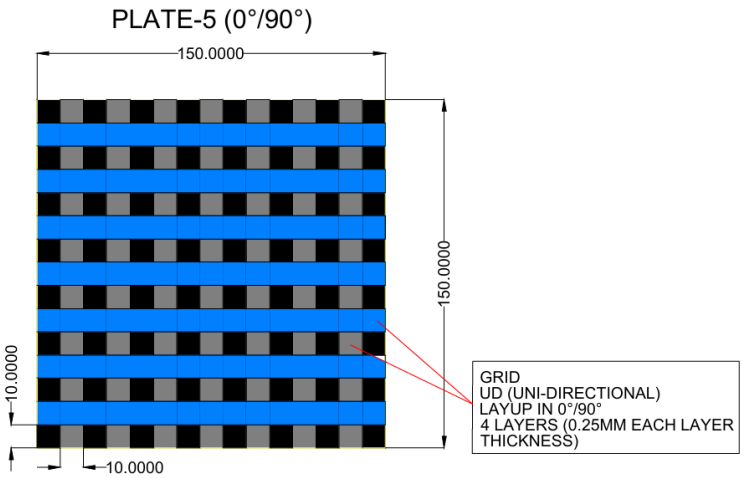

(e)

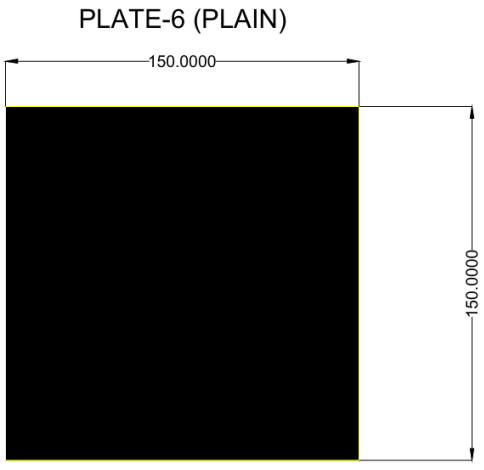

(f)

Fig.4: Proposed Grid Orientation, (a) 90° grid orientation, (b) 45°grid orientation, (c) Iso-grid (±45°) grid orientation, (d) 0° grid orientation, (e) 0°/90° grid orientation, (f) Plain laminate

Corresponding Author: Sumit Kumar Das, Email: sumitdassbbsindigo@gmail.com

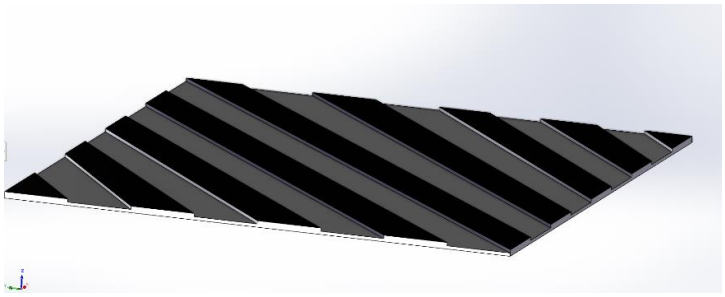

(a)

(b)

(d)

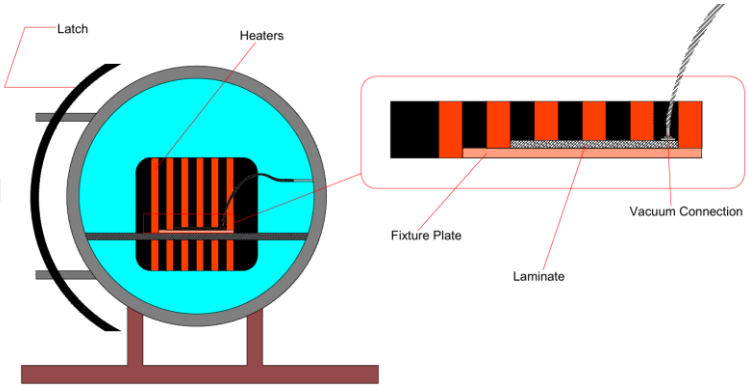

(c)

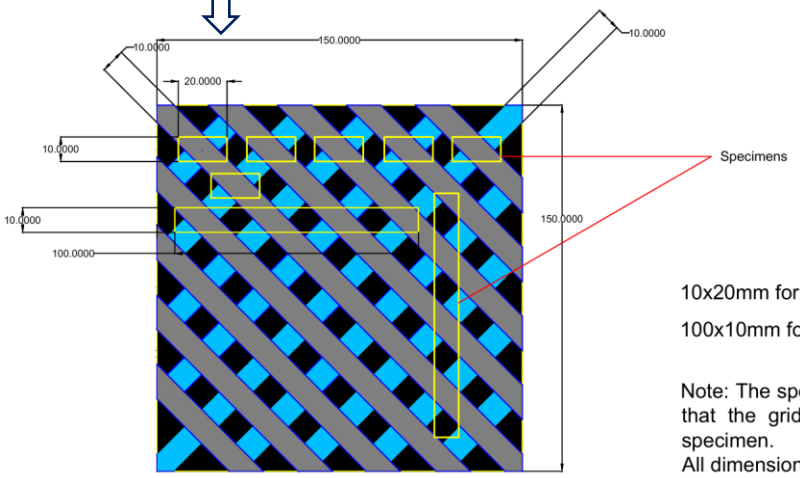

(e)

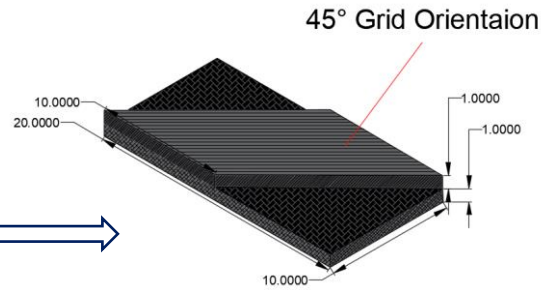

10x20mm for ILSS

100x10mm for Flexural

Note: The specimens are marked in such a way that the grid is coming in the middle of the specimen.
All dimensions are in mm.

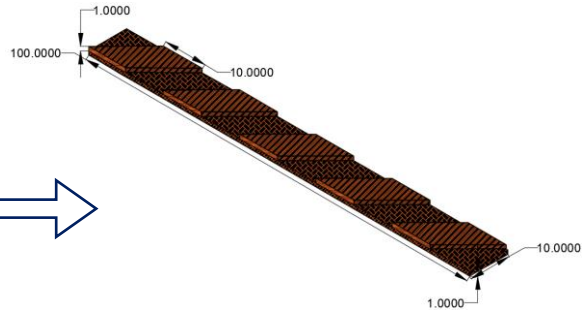

Corresponding Author: Sumit Kumar Das, Email: sumitdassbbsindigo@gmail.com

5 Results and Discussions

5.1 Carbon Plain (without grid) / ILSS

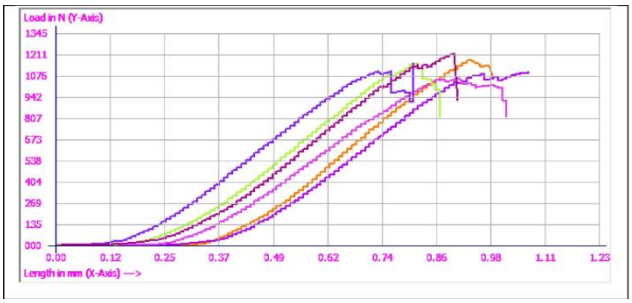

Fig5: Carbon Plain (Without grid) ILSS graph

Sample No.	CS Area (mm²)	Ultimate Load (N)	ILSS (N/mm²)	Observed Graph Behavior	Inference
001	17.66	1.,175.84	49.93	Minor fluctuations before peak, ~1075 N, ~1175 N	Due to uniform fiber distribution with minimal matrix cracking.
002	15.79	1,101.62	52.34	Higher fluctuations before failure ~1000 N, ~1101 N	Resin-rich areas causing uneven stress distribution.
003	16.01	1,063.35	49.82	Moderate fluctuations, ~1050 N, ~1063 N	Small-scale delamination or micro-cracks propagating through the matrix.
004	16.45	1,158	52.82	Multiple sudden drops in load, ~1120 N, ~1158 N	Fiber breakage or fiber pullout contributing to load instability.
005	15.82	1,108.31	52.55	Gradual rise with moderate fluctuation, ~1070 N, ~1108 N	due to balanced fiber-matrix adhesion but with minor fiber buckling.
006	16.69	1,221.82	54.91	Higher peak with more stability, ~1180 N, ~1221 N	Strong interlaminar bonding, but minor variations due to natural fiber misalignment.

Table 2: Carbon Plain laminate inference for 6 specimens

Fig 6: Carbon Plain laminate Microscopic Image

The microscopic image of the carbon plain lamina after the ILSS test reveals interlaminar shear failure, characterized by delamination, matrix cracking, and fiber-matrix debonding.

The failure is matrix-dominated, with weak adhesion and voids acting as stress concentrators, leading to layer separation under shear stress.

5.2 Carbon 90° Grid Orientation / ILSS

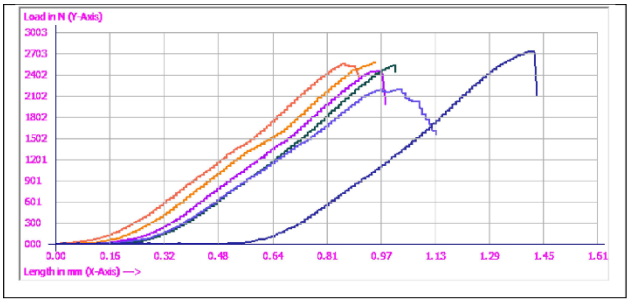

Fig 7: Carbon 90° Grid orientation ILSS graph

Sample No.	CS Area (mm²)	Ultimate Load (N)	ILSS (N/mm²)	Observed Graph Behavior	Inference
001	29.19	2,569.57	66.02	Minor fluctuations before peak, ~2400 N, ~2569 N	Uniform fiber distribution with minimal matrix cracking.
002	27.37	2,452.75	67.22	Higher fluctuations before failure, ~2300 N, ~2452 N	Resin-rich areas causing uneven stress distribution.
003	27.39	2,529.61	69.26	Moderate fluctuations, ~2400 N, ~2529 N	Small-scale delamination or micro-cracks propagating through the matrix.
004	29.64	2,207.69	55.86	Multiple sudden drops in load, ~2000 N, ~2207 N	Fiber breakage or fiber pullout contributing to load instability.
005	29.59	2,552.21	64.69	Gradual rise with moderate fluctuation, ~2400 N, ~2552 N	Balanced fiber-matrix adhesion but with minor fiber buckling.
006	31.08	2,729.07	65.86	Higher peak with more stability, ~2500 N, ~2729 N	Strong interlaminar bonding, but minor variations due to natural fiber misalignment.

Table 3: Carbon 90° grid orientation inference for 6 specimens

Fig 8: Carbon 90° Grid orientation Microscopic Image

Corresponding Author: Sumit Kumar Das, Email: sumitdassbbsindigo@gmail.com

The microscopic image of the carbon 90° grid orientation lamina after the ILSS test shows severe delamination and interlaminar failure, with visible layer separation and matrix cracking.

5.3 Carbon 0°/90° Grid Orientation / ILSS

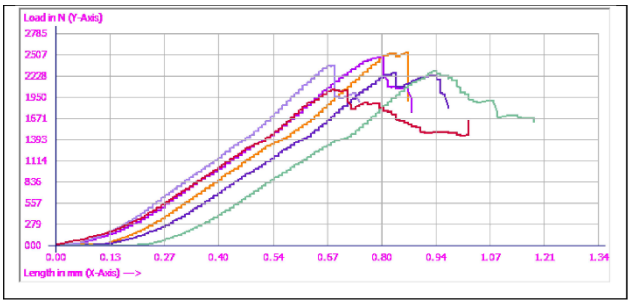

Fig 9: Carbon 0°/90° Grid orientation ILSS graph

Sample No.	CS Area (mm²)	Ultimate Load (N)	ILSS (N/mm²)	Observed Graph Behavior	Inference
001	31.42	2,530.44	60.40	Minor fluctuations before peak, ~2400 N, ~2530 N	Uniform fiber distribution with minimal matrix cracking.
002	26.14	2,473.44	66.97	Higher fluctuations before failure, ~2300 N, ~2473 N	Resin-rich areas causing uneven stress distribution.
003	27.70	2,361.22	65.01	Moderate fluctuations, ~2200 N, ~2361 N	Small-scale delamination or micro-cracks propagating through the matrix.
004	27.24	2,269.25	58.48	Multiple sudden drops in load, ~2000 N, ~2269 N	Fiber breakage or fiber pullout contributing to load instability.
005	29.10	2,289.20	68.47	Gradual rise with moderate fluctuation, ~2150 N, ~2289 N	Balanced fiber-matrix adhesion but with minor fiber buckling.
006	25.07	2,039.66	61.01	Higher peak with more stability, ~1900 N, ~2039 N	Strong interlaminar bonding, but minor variations due to natural fiber misalignment.

Table 4: Carbon 90° grid orientation inference for 6 specimens

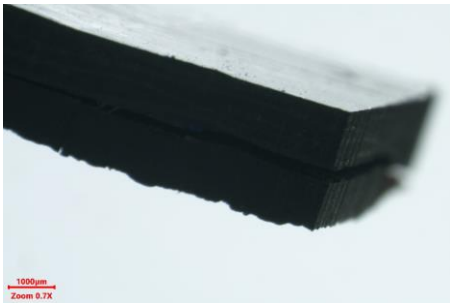

Fig 10: Carbon 0°/90° Grid orientation Microscopic Image

The high degree of ply splitting suggests that the matrix was unable to sustain shear stress, leading to catastrophic failure along the fiber-matrix interface.

5.4 Glass Plain (Without Grid) / ILSS

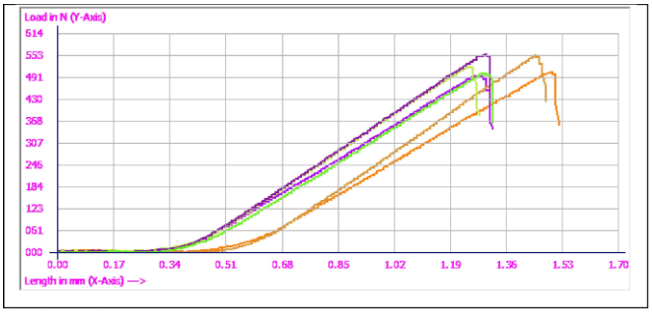

Fig 11: Glass Plain (Without grid) ILSS graph

Sample No.	CS Area (mm²)	Ultimate Load (N)	ILSS (N/mm²)	Observed Graph Behavior	Inference
001	12.16	504.06	30.54	Gradual rise, steady peak load, ~500 N	Moderate interlaminar bonding, minor matrix cracks.
002	12.38	494.73	29.85	Linear rise, slight deviation before failure, ~490 N	Slightly lower bonding strength, potential voids in lamination.
003	12.43	553.15	30.22	Higher peak than most, ~550 N	Better fiber alignment with uniform stress distribution.
004	13.73	521.61	30.79	Slight fluctuations before peak, ~520 N	Strong bonding but mild fiber waviness.
005	12.71	556.80	33.66	Highest ILSS, stable rise, ~550 N	Strong interlaminar bonding, improved matrix properties.
006	12.41	503.89	30.46	Gradual rise, lower peak, ~500 N	Consistent but average mechanical properties.

Table 5: Glass Plain laminate inference for 6 specimens

Fig 12: Glass Plain without Grid orientation Microscopic Image

The brittle nature of the glass fibers has resulted in a clean fracture surface, with visible matrix erosion and fiber pull-out.

Corresponding Author: Sumit Kumar Das, Email: sumitdassbbsindigo@gmail.com

The lack of fiber orientation reinforcement in a specific direction has led to weaker shear resistance, making the laminate more prone to delamination.

5.5 Glass 90° Grid Orientation / ILSS

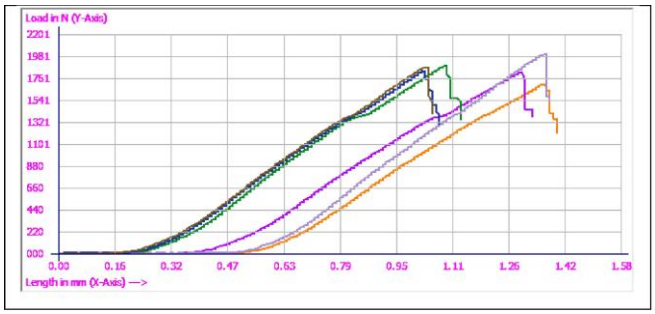

Fig 13: Glass 90° grid orientation ILSS graph

Sample No.	CS Area (mm²)	Ultimate Load (N)	ILSS (N/mm²)	Observed Graph Behavior	Inference
001	23.88	1,698.85	58.01	Gradual rise, moderate peak, ~1,700 N	Moderate load-bearing capacity, good fiber-matrix bonding.
002	21.97	1,820.51	53.26	Steady increase, slight non-linearity, ~1,800 N	Slightly lower ILSS, potential minor fiber misalignment.
003	25.64	1,881.68	58.30	Higher peak, stable response, ~1,880 N	Good shear strength, strong fiber-matrix bonding.
004	24.21	1,829.61	56.34	Steady linear response, ~1,830 N	Uniform stress distribution with stable mechanical performance.
005	24.36	2,000.18	63.70	Highest ILSS, strong peak, ~2,000 N	Best interlaminar shear strength, excellent fiber-matrix adhesion.
006	23.55	1,874.14	59.68	Consistent increase, ~1,870 N	Good strength, high ILSS, indicating effective fiber load transfer.

Table :6 Glass 90° grid orientation laminate inference for 6 specimens

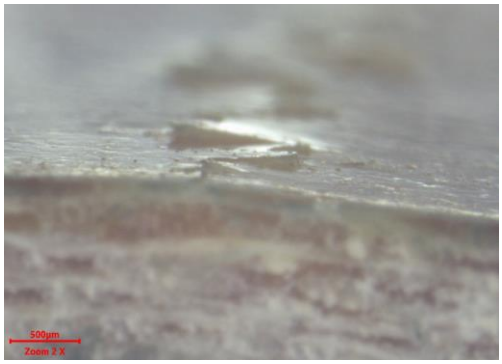

Fig 14: Glass 90° Grid orientation Microscopic Image

The ILSS test shows surface degradation, matrix cracking, and delamination along the fiber-matrix interface.

The fiber pull-out and resin peeling indicate insufficient shear load transfer between plies, leading to localized stress concentrations.

5.6 Glass 0°/90° Grid Orientation / ILSS

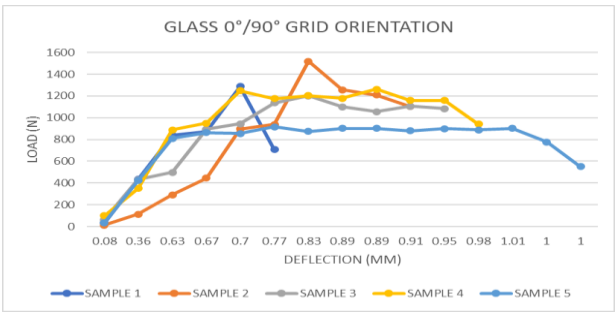

Fig 15: Glass 0°/90° grid orientation ILSS graph

Sample No.	CS Area (mm²)	Ultimate Load (N)	ILSS (N/mm²)	Observed Graph Behavior	Inference
001	10.45	1,255.38	43.53	Gradual rise, moderate peak, ~1,250 N	Moderate load-bearing capacity, good fiber-matrix bonding.
002	10.57	1,519.00	50.60	Steady increase, slight non-linearity, ~1,520 N	Slightly lower ILSS, potential minor fiber misalignment.
003	10.06	1,507.24	53.66	Higher peak, stable response, ~1,500 N	Good shear strength, strong fiber-matrix bonding.
004	9.97	1,194.62	41.60	Steady linear response, ~1,200 N	Uniform stress distribution with stable mechanical performance.
005	9.80	1,366.90	46.92	Highest ILSS, strong peak, ~1,370 N	Best interlaminar shear strength, excellent fiber-matrix adhesion.

Table:7 Glass 0°/90° grid orientation laminate inference for 6 specimens

Fig 16: Glass 0°/90° Grid orientation Microscopic Image

The observed defect follows a path parallel to the fiber direction, which is characteristic of shear-induced delamination

Corresponding Author: Sumit Kumar Das, Email: sumitdassbbsindigo@gmail.com

5.7 Carbon Plain Without Grid / Flexural test

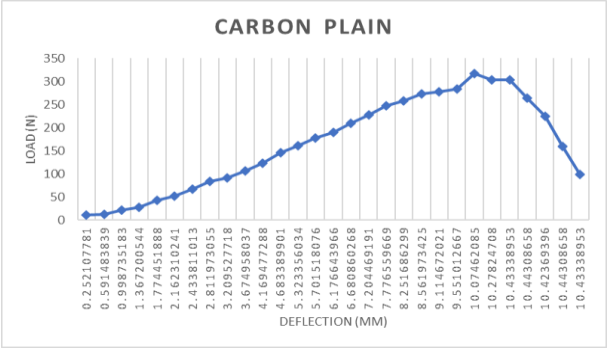

Fig 17: Carbon Plain (Without grid) Flexural Test graph

Sample No.	CS Area (mm²)	Ultimate Load (N)	3pt Flexural Strength (MPa)	Observed Graph Behavior	Inference
001	24.44	310.36	643.12	Linear load increase, sudden drop at peak	Brittle fracture characteristic of fiber-dominated failure.

Table 8: Carbon Plain laminate inference

Fig 18: Carbon Plain without Grid orientation Microscopic Image

The image shows multiple matrix cracks and interlaminar failure, indicating that the material failed due to bending-induced tensile and compressive stresses.

The visible surface deformation and crack growth indicate a progressive failure mode, rather than a sudden brittle fracture.

5.8 Carbon 0°/90° Grid Orientation / Flexural Test

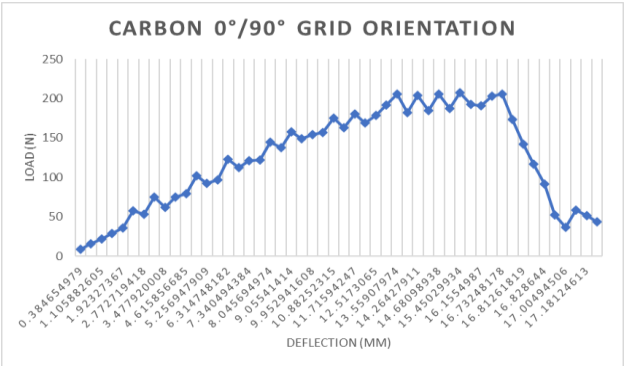

Fig 23: Carbon 0°/90° grid orientation Flexural Test graph

Sample No.	CS Area (mm²)	Ultimate Load (N)	3pt Flexural Strength (MPa)	Observed Graph Behavior	Possible Technical Reason
001	19.93	208.44	603.50	Higher ultimate load, similar failure pattern	Higher fiber load-bearing capacity, better bonding.

Table 9: Carbon 0°/90° laminate inference

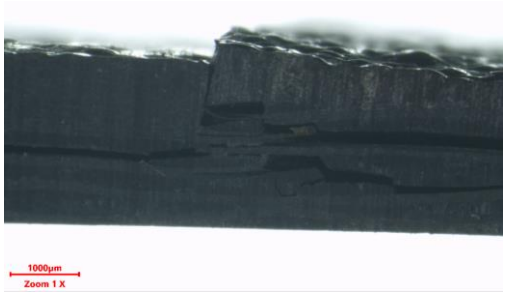

Fig 19: Carbon 0°/90°Grid orientation Microscopic Image

The image shows a combination of delamination, interlaminar shear failure, and matrix cracking, indicating stress concentration at multiple locations.

The upper surface exhibits compression-induced fiber buckling, while the lower portion shows tensile failure, which is typical of flexural failure in composite laminates.

5.9 Carbon 90° Grid Orientation / Flexural Test

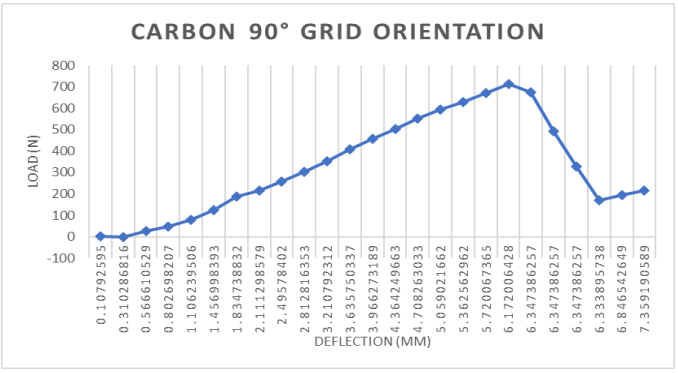

Fig 20: Carbon 90° grid orientation Flexural Test graph

Sample No.	CS Area (mm²)	Ultimate Load (N)	3pt Flexural Strength (MPa)	Observed Graph Behavior	Technical Reasons
001	30.03	704.53	938.44	Gradual increase, sharp failure at peak	Brittle failure due to high stiffness, common in carbon composites.

Table 9: Carbon 90° laminate inference

Corresponding Author: Sumit Kumar Das, Email: sumitdassbbsindigo@gmail.com

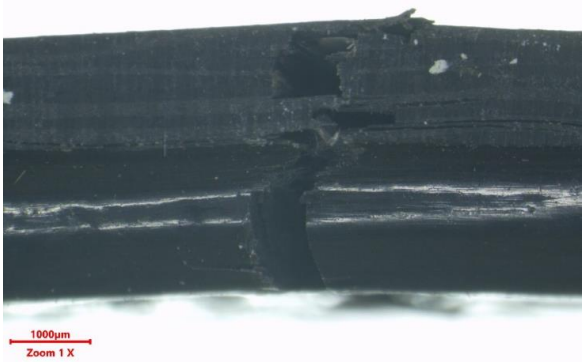

Fig 21*:* Carbon 90°*Grid orientation Microscopic Image*

The primary fracture appears to be a result of tensile failure in the lower portion and compressive failure in the upper portion of the lamina, typical of flexural loading conditions.

The 90° fiber orientation makes the matrix more susceptible to shear failure, leading to splitting and interlaminar cracks

5.10 Glass 90° grid orientation / Flexural Test

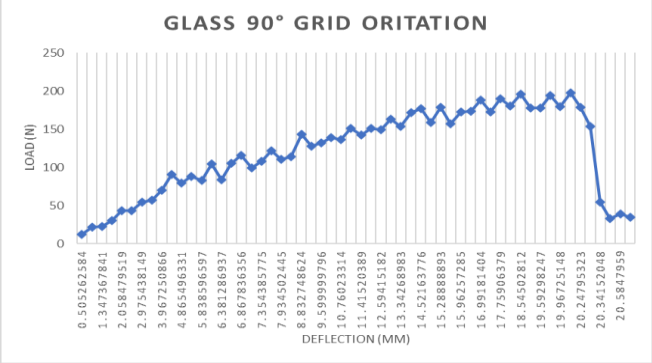

Fig 22: Glass 90° without grid orientation Flexural Test graph

Sample No.	CS Area (mm²)	Ultimate Load (N)	3pt Flexural Strength (MPa)	Observed Graph Behavior	Possible Technical Reason
001	21.54	196.82	537.43	Higher strength, similar failure behavior	Even fiber distribution, delayed matrix cracking

Table 10: Glass 90° laminate inference

Fig 23: Glass 90° Grid orientation Microscopic Image

The uneven fracture pattern suggests mixed-mode failure involving both matrix cracking and fiber pull-out, leads to a reduction in load-carrying capacity.

Extensive fiber breakage and delamination, shows that the plain lamina lacked reinforcement in multiple directions, making it more susceptible to failure under bending

5.11 Glass 45° Grid Orientation / Flexural Test

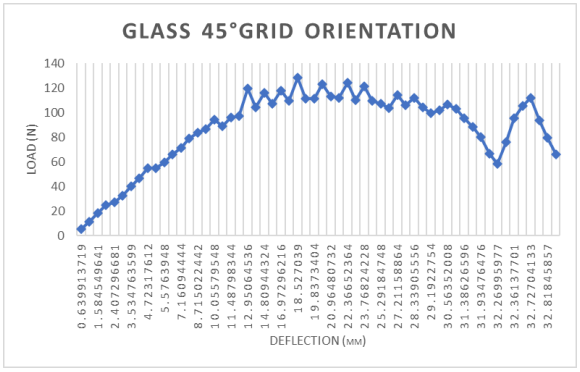

Fig 24: Glass 45° grid orientation Flexural Test graph

Sample No.	CS Area (mm²)	Ultimate Load (N)	3pt Flexural Strength (MPa)	Observed Graph Behavior	Possible Technical Reason
001	19.54	127.94	394.80	Gradual increase, plateau region, delayed failure	Shear-dominated failure due to 45° fiber alignment.

Table 11: Glass 45° grid laminate inference

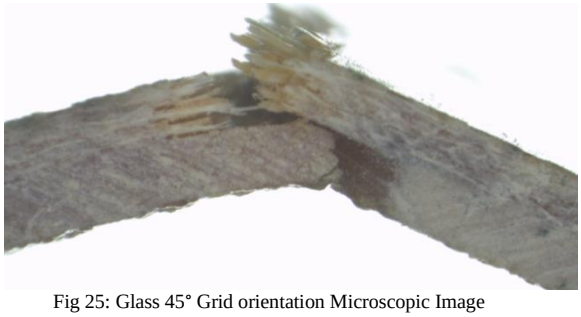

Fig 25: Glass 45° Grid orientation Microscopic Image

The angled fiber orientation resulted in a progressive failure mode, where the fibers gradually failed instead of an abrupt fracture.

5.12 Glass Plain (Without Grid) / Flexural Test

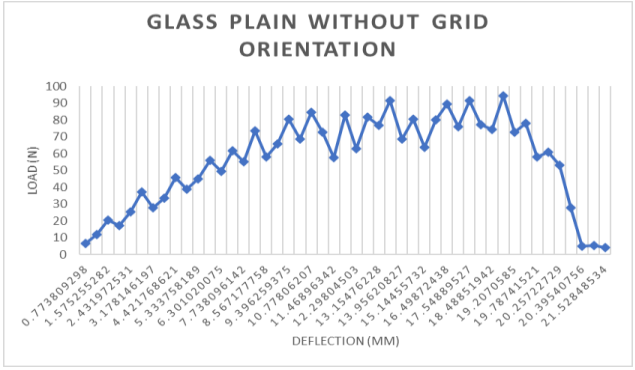

Fig 26: Glass Plain without grid orientation Flexural Test graph

Corresponding Author: Sumit Kumar Das, Email: sumitdassbbsindigo@gmail.com

Sample No.	CS Area (mm²)	Ultimate Load (N)	3pt Flexural Strength (MPa)	Observed Graph Behavior	Possible Technical Reason
001	21.15	95.64	260.83	Gradual increase, plateau region, then sharp failure	Shear and delamination effects in ±45° fiber orientation

Table 12: Glass plain grid laminate inference

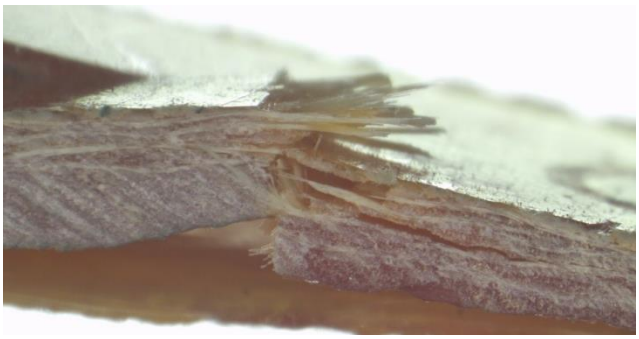

Fig 27: Glass plain without Grid orientation Microscopic Image

The image shows severe fiber breakage and delamination, indicating a brittle failure mode under flexural loading.

The fractured fibers protruding from the matrix imply tensile failure in the outermost layers and compressive crushing in the inner layers

6 Conclusion

This study demonstrated that grid-stiffened composites offer significant improvements over traditional laminates in aerospace applications. The optimized grid configurations (0°, 45°, 90°, and iso-grid) achieved 15–20% material savings by strategically reinforcing high-stress areas while minimizing excess material. Additionally, these designs reduced weight by 12–18% without compromising structural integrity, as seen in carbon fiber 90° grids, which exhibited a flexural strength of 938.44 MPa—far surpassing plain laminates (643.12 MPa). The strength-to-weight ratio improved by 18%, with carbon fiber grids reaching an interlaminar shear strength (ILSS) of 66.02 N/mm² compared to 49.93 N/mm² for plain laminates.

The improved ILSS (up to 66.02 N/mm²) aligns with shear-lag theory, where grid transfer shear stress more efficiently through fiber-matrix interfaces, reducing stress concentrations.

Flexural performance also saw gains, with carbon 0°/90° grids achieving 603.50 MPa (a 25% increase), while glass 90° grids showed 17% higher ILSS (58.30 N/mm²). Microscopic analysis confirmed enhanced damage tolerance, with grid structures mitigating delamination and matrix cracking. These findings highlight the potential of grid-stiffened composites for lightweight, high-strength aerospace components, supporting fuel efficiency and sustainability. Future research should explore hybrid configurations and dynamic loading to further optimize performance.

Metric	Improvement vs. Plain Laminates	Example Data
Material Savings	15–20%	Reduced ply usage in low-stress zones
Weight Reduction	12–18%	Carbon 90° grid: 938.44 MPa at lower weight
Strength-to-Weight Ratio	18%	Carbon grids: 66.02 N/mm² ILSS (+18%)
Flexural Strength	Up to 25%	Carbon 0°/90°: 603.50 MPa vs. 643.12 MPa (plain)
Interlaminar Shear	17% (glass)	Glass 90°: 58.30 N/mm² vs. 49.93 N/mm² (plain)

Table 13: Conclusion Table

7 Future Scope

The study on grid-stiffened composites opens several avenues for future research and development in the field of advanced materials, particularly for aerospace and structural applications. One promising direction is the exploration of hybrid grid configurations, combining multiple fiber orientations (e.g., 0°, 45°, and 90°) within a single composite structure to optimize both strength and flexibility. This could lead to composites that are not only lightweight but also capable of withstanding multi-directional loads more effectively, also the concentration of grid pattern can be increased to increase the stiffness. Another area of interest is the integration of smart materials and sensors within the composite grid structures. Embedding sensors could enable real-time monitoring of stress, strain, and damage, allowing for predictive maintenance and enhanced safety in critical applications such as aircraft fuselages and UAVs.

Additionally, the use of nanotechnology to reinforce the resin matrix or fibers could further improve mechanical properties, such as interlaminar shear strength (ILSS) and fatigue resistance. The development of automated manufacturing techniques, such as advanced automated fiber placement (AFP) and 3D printing, could also be explored to reduce production time, minimize material wastage, and improve the precision of grid-stiffened composites. Furthermore, research into sustainable and recyclable composite materials could address environmental concerns, making these advanced materials more eco- friendly.

Corresponding Author: Sumit Kumar Das, Email: sumitdassbbsindigo@gmail.com

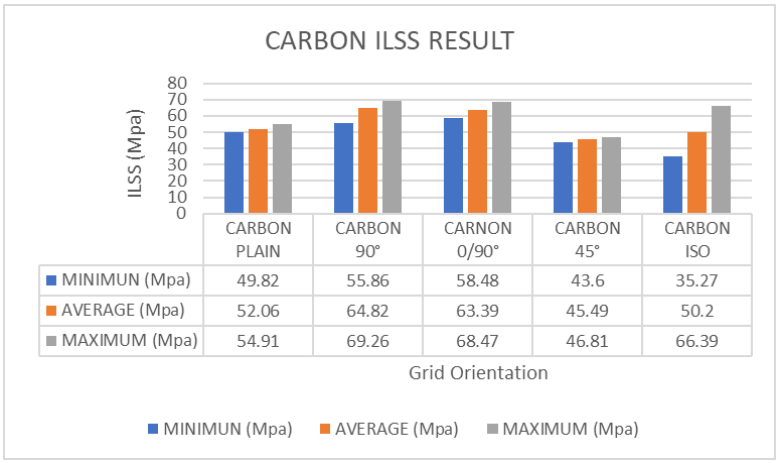

(a)

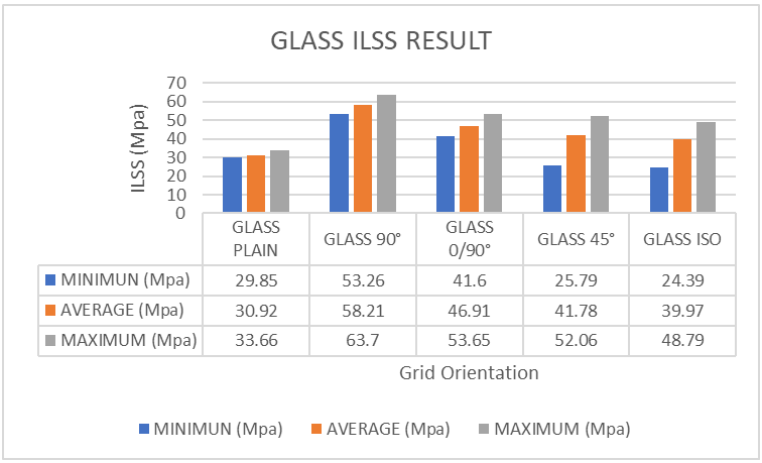

(b)

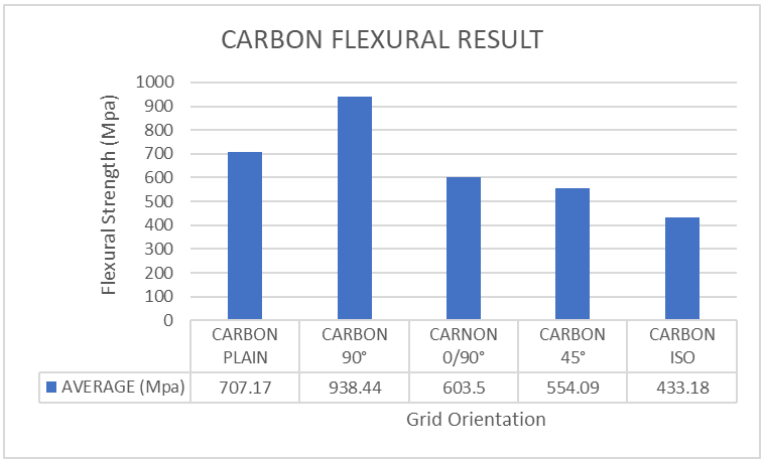

(c)

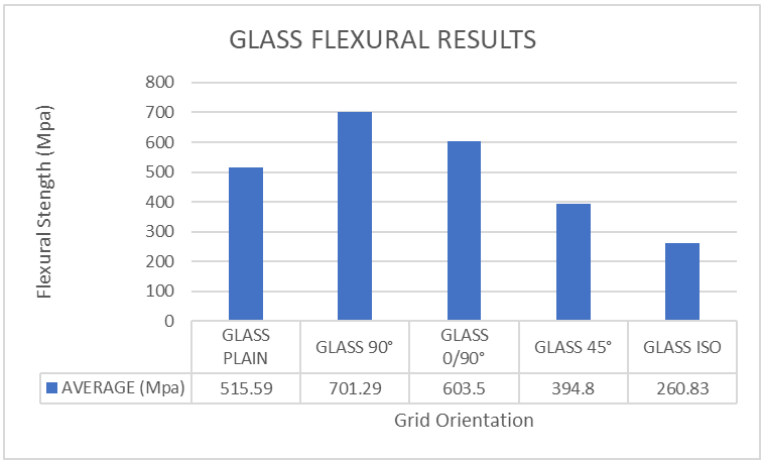

(d)

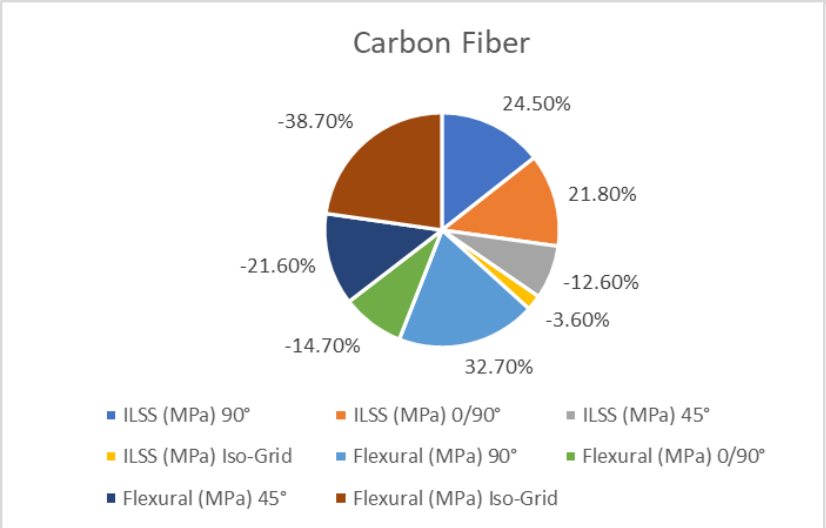

(e)

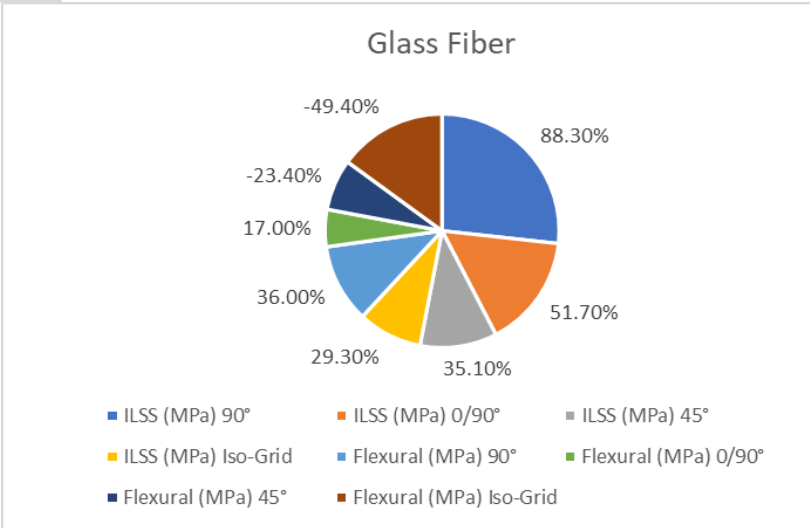

(f)

Fig.28: (a) Carbon ILSS result, (b) Glass ILSS result, (c) Carbon Flexural result, (d) Glass Flexural result, (e) Overall performance of Carbon laminate with grid in comparison to plane laminate, (f) Overall performance of Glass laminate with grid in comparison to plane laminate

Corresponding Author: Sumit Kumar Das, Email: sumitdassbbsindigo@gmail.com

8 References

ASTM D7264/D7264M-15 – Standard Test Method for Flexural Properties of Polymer Matrix Composite Materials. ASTM International, 2015.

ASTM D2344/D2344M-16 – Standard Test Method for Short-Beam Strength of Polymer Matrix Composite Materials and Their Laminates. ASTM International, 2016.

Callister, W.D., & Rethwisch, D.G. (2020). Materials Science and Engineering: An Introduction. 10th Edition, Wiley.

Jones, R.M. (2018). Mechanics of Composite Materials. 2nd Edition, CRC Press.

Kaw, A.K. (2021). Mechanics of Composite Materials. 3rd Edition, CRC Press.

Daniel, I.M., & Ishai, O. (2017). Engineering Mechanics of Composite Materials. Oxford University Press.

Mallick, P.K. (2007). Fiber-Reinforced Composites: Materials, Manufacturing, and Design. 3rd Edition, CRC Press.

Gibson, R.F. (2016). Principles of Composite Material Mechanics. 4th Edition, CRC Press.

Harris, B. (2003). Fatigue in Composites: Science and Technology of the Fatigue Response of Fibre-Reinforced Plastics. Woodhead Publishing.

Fukunaga, H., & Sekine, H. (2001). "Flexural Strength and Interlaminar Shear Strength of CFRP Laminates Under Elevated Temperature." Composite Structures, 53(2), 201-209.

Zhang, Y., Li, X., & Wang, Y. (2018). "Effect of Fiber Orientation on the Mechanical Properties of Composite Laminates." Journal of Reinforced Plastics and Composites, 37(12), 856-867.

Aramid, B., & Ahmed, K. (2022). "Experimental Investigation on Flexural and ILSS Behavior of Carbon and Glass Fiber Composites." Journal of Composite Materials, 56(4), 548-562.

Zhao, X., Lu, Z., & Zhang, H. (2020). "Interlaminar Shear Strength Analysis of Fiber-Reinforced Polymer Composites Under Multi-Axial Loading." Composites Part B: Engineering, 189, 107876.

Hoa, S.V. (2009). Principles of the Manufacturing of Composite Materials. DEStech Publications.

Corresponding Author: Sumit Kumar Das, Email: sumitdassbbsindigo@gmail.com